Optical-Feedback-Induced Chaos and its Control in Multimode Semiconductor Lasers

Andrew T. Ryan, Govind P. Agrawal, *Senior Member, IEEE*, George R. Gray, *Member, IEEE*, and Edward C. Gage

Abstract—**The effects of optical feedback in multilongitudinal mode semiconductor lasers are studied through computer simulations. Two separate regimes are found based on the length of the external cavity. For long external cavities (external-cavity mode spacing larger than the relaxation-oscillation frequency), the laser follows a quasi-periodic route to chaos as feedback is increased. For short external cavities, the laser can undergo both quasi-periodic and period doubling routes to chaos. When the laser output becomes chaotic, the relative-intensity noise is greatly increased (by more than 20 dB) from its solitary-laser value. Considerable attention is paid to the effects of optical feedback on the longitudinal-mode spectrum. The stabilization of the mode spectrum and the reduction of the feedback-induced noise through current modulation are studied and compared with experimental results. Current modulation eliminates feedback-induced chaos when the modulation frequency and depth are suitably optimized. This technique of chaos control has applications in optical data recording.**

I. Introduction

IN MANY applications, such as optical data recording and fiber-optic communication systems, semiconductor lasers operate in the presence of external optical feedback (OFB). It has been observed that even small amounts of OFB can affect the laser behavior dramatically [1]–[15]. At relatively low OFB levels (<-40 dB) the effect of OFB can be beneficial since it can be used for linewidth narrowing. However, when the OFB level exceeds a critical value (~-40 dB), the laser enters a so-called coherence collapse regime [3] in which the laser linewidth increases by orders of magnitudes (from <100 MHz to >10 GHz). At the same time, the low-frequency relative-intensity noise (RIN) can be greatly enhanced (by >20 dB), a feature that drastically degrades system performance. Considerable work done over the last few years [3]–[15] has revealed that coherence collapse is associated with a transition from the continuous-wave (CW) state to a chaotic state, often following a quasi-periodic route to optical chaos [15]. However, most of the previous work has used a single-mode rate-equation model, and therefore applies, strictly speaking, to semiconductor lasers oscillating predominantly in a single-longitudinal mode (e.g., a distributed feedback laser). Many practical applications (such as optical data recording and optical data links) normally use Fabry–Perot-type semiconductor lasers operating in several longitudinal modes simultaneously. It is thus of practical importance to investigate the coherence-collapse region in multimode semiconductor lasers.

The objective of this paper is two-fold. First, we use a multimode rate-equation model to study the effect of OFB on the performance of multimode semiconductor lasers and compare the results with those obtained for a single-mode laser. We show that the transition to optical chaos at a critical OFB level can occur following both a period-doubling route and a quasi-periodic route depending on the feedback parameters such as the external-cavity length. Second, we investigate how optical chaos can be controlled by using current modulation, a technique referred to as high-frequency injection (HFI) in the optical data recording literature [16]–[22]. It has been observed experimentally [18]–[20] that modulation of the driving current suppresses the feedback-induced RIN enhancement when the modulation frequency and the amplitude are suitably chosen. However, the optimum values of the modulation frequency and amplitude need to be determined empirically since a theoretical understanding has been lacking. Our multimode rate-equation model is capable of explaining why the RIN is increased and why this increase can be avoided through high-frequency injection [22]. Computer simulations are used to find the optimum parameters for controlling the laser-intensity noise. The results are compared with the experimental data.

In the next section we present the multimode rate-equation model. Section III focuses on the single-mode case in order to establish a relation to previous work. However, in contrast with most of the previous work, we also consider the case of short external cavities, for which the external-cavity mode spacing is considerably above the relaxation-oscillation frequency of the laser. Our numerical simulations show the existence of both period-doubling and quasi-periodic routes to chaos for such short external cavities. In the opposite case in which the external cavity is so long that the external-cavity mode spacing is considerably below the relaxation-oscillation frequency, optical chaos occurs through the quasi-periodic route, as also observed experimentally [15]. In Section IV we consider chaos in a multimode semiconductor laser and compare it with the single-mode case. An important result is related to the possibility of mode switching in multimode lasers. Even though almost all of the power is carried by a single dominant mode in the chaotic state, the dominant mode is not always the same. Section V discusses the feedback-induced mode hopping

Manuscript received Jan. 18, 1993; revised June 7, 1993. This work is supported by the New York State Center for Advanced Optical Technology and the U.S. Army Research Office.

A. T. Ryan and G. P. Agrawal are with The Institute of Optics, University of Rochester, Rochester, NY 14627 USA.

G. R. Gray is with the Electrical Engineering Department, University of Utah, Salt Lake City, UT 84112 USA.

E. C. Gage is with Eastman Kodak Company, Rochester, NY 14652 USA.

IEEE Log Number 9215349.

by including the effects of spontaneous emission on the chaotic dynamics of multimode lasers. The control of chaos through current modulation is considered in Section VI where we also discuss the applications of this technique in optical data recording. Section VII compares the numerical results with the experimental data obtained by using a 780-nm GaAlAs laser. The main results of the paper are summarized in the concluding section.

II. Multimode Rate-Equation Model

The dynamic and noise characteristics (such as the RIN, the frequency noise, and the spectral linewidth) can be studied by using a rate-equation model that includes the effect of spontaneous-emission noise and shot noise through a random term added to each rate equation [1], [2]. The effects of optical feedback and current modulation can also be included in this model in a straightforward manner by generalizing the model of Lang and Kobayashi [23]. In the general case of a multimode semiconductor laser, these rate equations can be written as [22]

$$\frac{dE_m}{dt} = -\tfrac{1}{2}(1-i\alpha)(G_m-\gamma_m)E_m + \zeta_m^{\text{int}} + F_m(t) + \kappa_m E_m(t-\tau)\exp(i\omega_m\tau) \quad (1)$$

$$\frac{dN}{dt} = \frac{I}{q} - \frac{N}{\tau_e} - \sum_{j=1}^{M} G_j|E_j|^2 + F_N(t) \quad (2)$$

where

$$G_m(N) = A(N-N_0) - \delta G_m \quad (3)$$

$$\zeta_m^{\text{int}} = -\tfrac{1}{2}\left(\beta_m P_m + \sum_k \theta_{mk}P_k\right)E_m + \sum_k \kappa_{mk}E_{2k-m}^* E_k^2. \quad (4)$$

In (1) $E_m(t)$ is the complex amplitude of the mth mode oscillating at the frequency ω_m, G_m is the mode gain, γ_m is the mode-dependent cavity loss, ζ_m^{int} accounts for interaction among laser modes through various processes such as self-saturation, cross saturation, and four-wave mixing, $\tau = 2L_{\text{ext}}/c$ is the round-trip time in the external cavity of length L_{ext}, and $F_m(t)$ accounts for the random noise generated through spontaneous emission. The complex electric field is written in terms of amplitude and phase as $E_m = \sqrt{P_m}\,e^{-i\phi}$, where P_m and ϕ are the photon number and phase, respectively, of the mth mode. In (2) N is the electron number inside the active region of the semiconductor laser, I is the injection current, q is the magnitude of the electron's change, τ_e is the carrier lifetime, and $F_N(t)$ is a random noise term to account for carrier generation and recombination (shot noise). In (3) and (4), A is the gain parameter related to the rate at which the peak gain increases with increasing N, N_0 is the transparency value of N, δG_m is the gain margin related to the offset of the mode from the gain peak, β_m is the self-saturation parameter, θ_{mk} is the cross-saturation parameter, and κ_{mk} is the four-wave-mixing parameter. The numerical values of β_m, θ_{mk}, and κ_{mk} depend on the mechanism responsible for the mode interaction. Their expressions are well known for the case in which the mode interaction occurs due to intraband nonlinearities related to spectral hole-burning [24]. Other mechanisms such as carrier heating and mode beating can be easily included. Although four-wave-mixing coupling is included in (1), we neglect such coupling for this paper, since its effect is expected to be small. The self-saturation parameter β_m is related to the commonly used nonlinear-gain parameter ϵ as $\beta_m = \epsilon\gamma_m/V_m$, where V_m is the mode volume. We assume β_m to be the same for all modes.

The effect of optical feedback is included through the last term in (1). The feedback parameter κ_m is given by [23]

$$\kappa_m = \frac{(1-R_f)}{\tau_{Lm}}\sqrt{\frac{\eta_{cm}R_{\text{ext}}}{R_f}} \quad (5)$$

where R_{ext} is the fraction of output power that is reflected back toward the laser facet of reflectivity R_f facing the external cavity, τ_{Lm} is the round-trip time of the mth mode in the laser cavity, and η_{cm} is the coupling efficiency of the returned light into the active region. Both τ_{Lm} and η_{cm} are nearly the same for all modes, and can be assumed to be mode-independent to a good approximation. In contrast, the phase shift $\omega_m\tau$ in the external cavity is not the same for all modes because of their different frequencies ω_m. It is useful to write ω_m as

$$\omega_m = \omega_c + (m-m_0)\Delta\omega_L \quad (6)$$

where ω_c is the angular frequency of the central mode located at $m = m_0$, and $\Delta\omega_L/2\pi$ is the longitudinal-mode spacing ($\sim$100 GHz). For the purpose of numerical simulations, we define F_{ext} as $F_{\text{ext}} = \eta_c R_{\text{ext}}$ and assume it to be mode independent since the coupling efficiency η_c (typically $\sim$1–5%) is nearly the same for all longitudinal modes of the laser. Physically, F_{ext} represents the fraction of output power that reenters the laser cavity.

The rate equations (1) and (2) can be used to obtain the RIN of the diode laser in the presence of optical feedback by calculating the spectrum of intensity fluctuations. If $P_m(t)$ is the mth mode photon number, and $\overline{P}_m$ is its average value, the RIN spectrum is defined as the Fourier transform of the autocorrelation function according to the relation

$$S_m(\omega) = \frac{1}{\overline{P}_m^2}\int_{-\infty}^{\infty}\langle\delta P_m(t)\delta P_m(t+t')\rangle\exp(-i\omega t')\,dt' \quad (7)$$

where $\delta P_m(t) = P_m(t) - \overline{P}_m$ is the fluctuation at time t. Equation (7) provides RIN for a specific laser mode. The RIN for the total photon number is obtained by replacing P_m by P_T in (7), where $P_T(t) = \Sigma_{m=1}^{M} P_m(t)$. The photon number can be converted to the optical power by using the well-known relation given, for example, in [1] and [2].

In the remaining sections we present the results obtained by integrating the rate equations (1) and (2) numerically using a fourth-order Runge–Kutta algorithm. The parameter values used correspond to a typical index-guided GaAlAs semiconductor laser likely to be used in optical recording systems. These values are listed in Table I, and result in a threshold current of 61 mA and a slope efficiency of about 0.5 mW/mA. The external mirror (optical disk in the case of data recording systems) is facing the low-reflectivity mirror. Most

TABLE I
TYPICAL PARAMETER VALUES OF LASER USED IN NUMERICAL SIMULATIONS FOR A 780-nm GaAlAs SEMICONDUCTOR LASER

Parameter	Symbol	Value
Laser cavity length	L	350 μm
Solitary-laser round-trip time	τ_L	9.3 ps
Linewidth enhancement factor	α	4
Laser facet reflectivities	R_1, R_2	0.9, 0.12
Mode loss rate (using internal loss of 65 cm^{-1})	γ_m	$7.26 \cdot 10^{11}$ s^{-1}
External-cavity length	L_{ext}	10 cm
External-cavity round-trip time	τ	0.67 ns
Carrier recombination time	τ_e	2 ns
Gain coefficient	A	$1.19 \cdot 10^3$ s^{-1}
Transparency carrier number	N_0	$1.64 \cdot 10^8$
Spontaneous emission factor	n_{sp}	1.8
Nonlinear-gain parameter	ϵ	$4 \cdot 10^{-18}$ cm^3
Self-saturation coefficient	β_m	$4.7 \cdot 10^3$ s^{-1}
Cross-saturation coefficient	θ_{mk}	$4.4 \cdot 10^3$ s^{-1}
Bias current	I_b	65 mA
Average output power	P_{out}	1.6 mW
Coupling efficiency	η_c	2%

of the simulations are presented for a constant laser power of 1.6 mW, which is a typical value used for reading data from an optical disk in optical data recording systems. We include five longitudinal modes in our numerical simulations. The RIN spectra are calculated from time series of lengths 30–500 ns, depending on the resolution desired, after the transients have died out. The spectra are averaged over several trajectories to improve numerical accuracy.

III. CHAOS IN SINGLE-MODE SEMICONDUCTOR LASERS

As mentioned in the Introduction, we first present results describing the chaotic dynamics of single-mode semiconductor lasers in the presence of OFB. For chaos occurring in single-mode lasers with, in particular, long external cavities, the use of bifurcation diagrams and Poincaré sections to describe the behavior is well established [15]. We begin by showing a series of bifurcation diagrams to point out the differences between long and short external cavities. Figure 1 presents bifurcation diagrams for a single-mode laser (as with all of the following results, except where specified, the laser is described by the parameters in Table I) for external cavity lengths L_{ext} in the range 10–100 cm. These bifurcation diagrams were obtained by generating a time series for each OFB level, and then noting the carrier number N when the laser intensity crossed the solitary-laser value. The random noise terms have been neglected in making these diagrams, so that we may separate the deterministic effects from stochastic effects. The parameter F_{ext} is varied over a wide range (40 dB) covering 10^{-6} to 10^{-2}. The feedback phase $\omega_0\tau$ is set to zero and was kept fixed at this value in all simulations. The feedback phase is known to play an important role and can affect the laser linewidth considerably [6]–[9]. However, in optical recording systems this phase cannot be chosen to minimize the laser linewidth since its exact value is somewhat arbitrary. Even though this phase is expected to stay constant during a single bit, its value is likely to change from bit to bit because of disk-surface imperfections. The results presented here and the conclusions drawn are nearly insensitive to the value of feedback phase used in numerical simulations.

Figure 1(a) corresponds to a relatively long cavity (L_{ext} = 100 cm). It shows a quasi-periodic route to chaos, in agreement with previous work [15]. However, for L_{ext} = 30 cm [Fig. 1(b)] the laser output becomes chaotic by following a period-doubling route. Two period-doubling bifurcations occurring at approximately $F_{ext} = 3.5 \cdot 10^{-6}$ and $6 \cdot 10^{-6}$ are clearly evident, followed by full-blown chaos after $F_{ext} = 1.5 \cdot 10^{-5}$. While the two cases demonstrate two different routes to chaos, they share the common feature that chaotic behavior persists over a wide range of F_{ext} without stable windows of CW or periodic operation. This is the defining feature of the long-cavity regime in which the external-cavity mode spacing ν_{ext} exceeds the relaxation-oscillation frequency ν_R (about 700 MHz at 1.6-mW output power). Such a low value of the relaxation frequency is common in optical recording systems during the reading operation since the laser output power is kept low.

The qualitative behavior changes considerably in the short-cavity limit defined by the condition $\nu_{ext} > \nu_R$. For our laser this condition is satisfied for $L_{ext} < 21$ cm. Figure 1(c) shows the bifurcation diagram for the same laser, but with an external cavity length of 15 cm. The most important qualitative difference is that chaos is interrupted by multiple windows of stability as F_{ext} increases. The stable windows become wider when L_{ext} decreases further. This is evident in Fig. 1(d), which shows the bifurcation diagram for L_{ext} = 10 cm. The laser enters the first chaotic window through a period-doubling route at approximately $F_{ext} = 2 \cdot 10^{-5}$, but chaos gives way to a CW steady state when F_{ext} exceeds $6 \cdot 10^{-5}$. It enters a second chaotic region for $F_{ext} > 1.5 \cdot 10^{-4}$. This scenario is repeated many times. However, the route to chaos is the quasi-periodic type for higher OFB levels. Thus, the same laser can exhibit a period-doubling or a quasi-periodic route depending on the OFB level. We note that different chaotic windows in Figs. 1(c) and 1(d) are of roughly the same size when F_{ext} is plotted on a linear scale. Further reduction in the external cavity length makes the laser less and less chaotic. Eventually the chaos disappears for cavity lengths shorter than 0.5 cm, a feature in agreement with the experiments and previous theoretical work [6].

The location and width of the chaotic and stable windows in Fig. 1 depend on many laser parameters. Extensive numerical simulations indicate that the two most important parameters from the chaos standpoint are the linewidth enhancement factor α and the nonlinear gain parameter ϵ. The sensitivity on ϵ is not surprising since the damping rate of relaxation oscillations in semiconductor lasers is mostly governed by the nonlinear gain. Optical chaos sets in when the OFB reduces the damping rate to the extent that relaxation oscillations become undamped. Since an increase in ϵ makes the steady state more stable by increasing the damping rate of relaxation oscillations, one would expect chaos to occur at higher OFB levels for larger values of ϵ. Numerical results confirm this behavior. Figure 2 shows a bifurcation diagram for L = 10 cm under

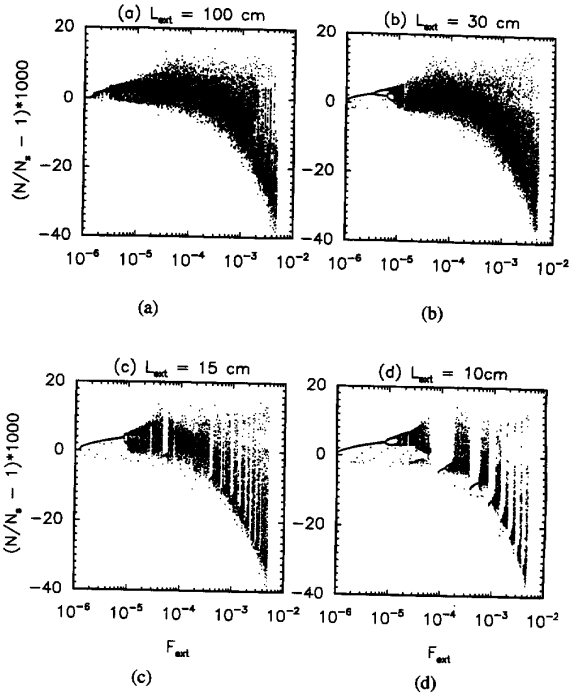

Fig. 1. Bifurcation diagrams showing the carrier number N (normalized to the solitary-laser value N_s) as a function of F_{ext} for a single-mode semiconductor laser for L_{ext} in the range 10–100 cm. The other parameter values are given in Table I.

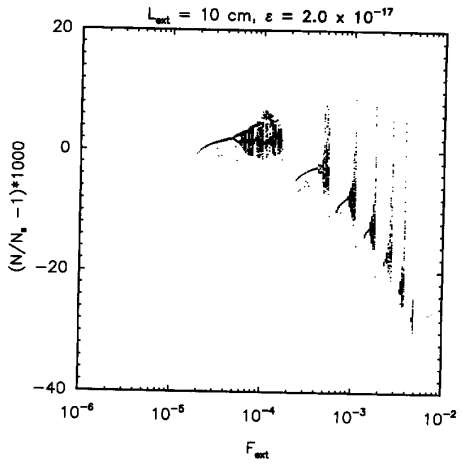

Fig. 2. Bifurcation diagram for $L_{\text{ext}} = 10$ cm when the nonlinear gain is increased to $\epsilon = 2 \cdot 10^{-17}$ cm^{-3}.

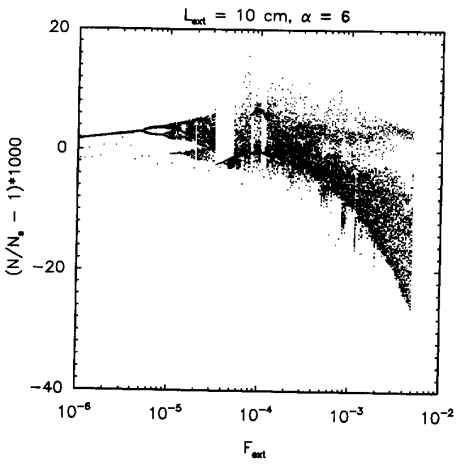

Fig. 3. Bifurcation diagram for $L_{\text{ext}} = 10$ cm when the linewidth enhancement factor is increased to $\alpha = 6$.

the same conditions of Fig. 1(d) expect that $\epsilon = 1 \cdot 10^{-17}$ cm^{-3}. A comparison of Figs. 1(d) and 2 reveals that for larger values of ϵ not only does the chaos set in at higher OFB levels, but also the location and width of chaotic windows differ greatly. The white region in Fig. 2 for $F_{\text{ext}} < 2 \cdot 10^{-5}$ corresponds to the steady-state operation of the laser, in which the laser operates at a constant power different from that of the solitary laser. This region is much wider for a larger value of ϵ since the relaxation oscillations are more difficult to destabilize in that case.

The dependence of chaotic dynamics on the linewidth enhancement factor α is also quite dramatic. In general, chaos is helped by larger values of α. Indeed, the laser remains stable and does not exhibit chaos when α is below a critical value that depends on many other parameters (typically $\alpha_{\text{crit}} < 1$). By contrast, chaos becomes much more dominant for large values of α. Figure 3 shows the bifurcation diagram under conditions identical to those of Fig. 1(d) except that α has been increased from 4 to 6. A comparison of Figs. 1(d) and 3 shows that the stable windows have almost disappeared for $\alpha = 6$. At the same time, there is evidence of a second chaotic attractor [15]. The dependence of the chaotic behavior on α can be understood by noting that the parameter α governs the amplitude-phase coupling in semiconductor lasers. Since light fed back into the laser cavity is delayed in the external cavity, the OFB makes the laser much more sensitive to changes in the optical phase (OFB acts as a memory device because of its delayed nature). Any phase changes are then transformed to gain changes with proportionality constant α. In the next section we study how changing the number of modes impacts the chaotic dynamics.

IV. Chaos in Multimode Semiconductor Lasers

The chaotic dynamics of multimode semiconductor lasers was studied by considering five longitudinal modes. The cross-saturation parameter was chosen such that all five modes were above threshold for the solitary laser when spontaneous emission was included. In the absence of spontaneous emission, even a multimode laser can have almost all of its power in a single longitudinal mode when the steady state is reached. One may think naively that the differences between the single- and multimode cases would be negligible in that case. However, the results of this section show that this is not the case. The reason is that when the steady state becomes unstable, the laser has the possibility of sharing its power with

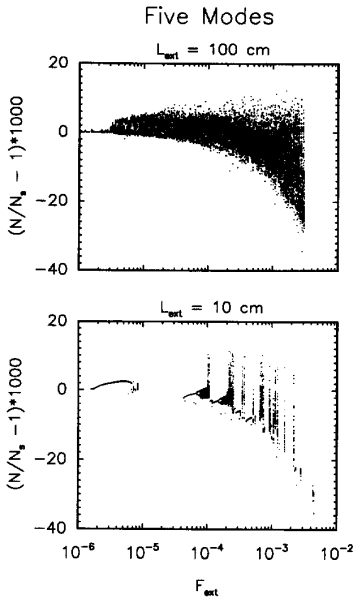

Fig. 4. Bifurcation diagram for $L_{\text{ext}} = 10$ and 100 cm for a multimode semiconductor laser (with 5 modes). The other parameter values are identical to the single-mode case (see Table I).

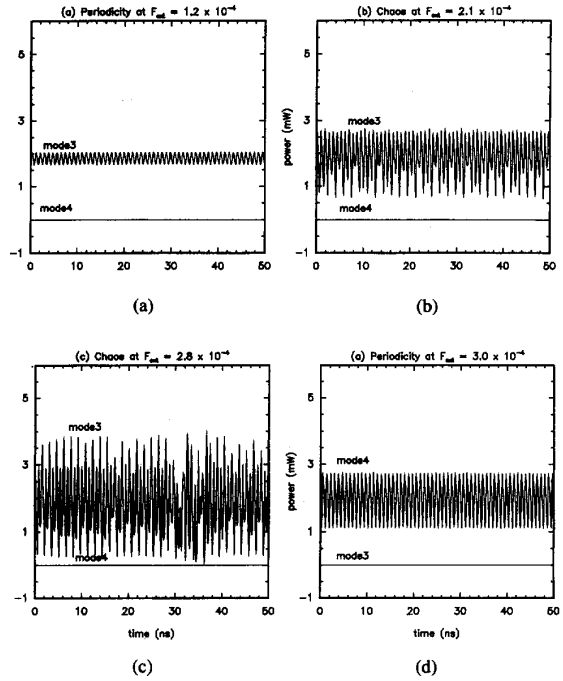

Fig. 5. Temporal variation of mode powers for two neighboring modes at four levels of feedback, showing the onset of chaos and then the transition to a periodic state through mode switching.

other longitudinal modes, a possibility that does not exist in single-mode simulations. Similar to the single-mode case, a distinction can be made between the short- and long-cavity regimes. Figure 4 shows the bifurcation diagrams (made when the total power P_T crosses its solitary value) for $L_{\text{ext}} = 10$ and 100 cm. As in the single-mode case, chaos persists over a wide range of F_{ext} for long external cavities, but is interrupted by windows of stable regions in the case of short L_{ext}. A comparison of Figs. 1(a) and 4(a) shows that the differences between the single-mode and multimode cases are relatively minor in the case of long cavities ($\nu_{\text{ext}} > \nu_R$). In the following discussion we concentrate on the short-cavity case.

A comparison of Figs. 1(d) and 4(b) reveals the effect on the chaotic dynamics of having multiple longitudinal modes. The qualitative differences in the single-mode and multimode cases are quite evident. In the multimode case the onset of full-blown chaos is delayed by a factor of 10 relative to the single-mode case. It appears that multimode lasers are less sensitive to OFB than their single-mode counterparts for a given set of device parameters. This result can be understood qualitatively by noting that all modes contribute to the damping of relaxation oscillations. Thus, even though individual modes may become unstable in isolation, simultaneous lasing of all modes preserves the steady state over a larger range of F_{ext}. Figure 4(b) shows that the CW state first becomes unstable and the total output power becomes periodic (at the relaxation-oscillation oscillation frequency ν_R) at a small OFB level of about $1.5 \cdot 10^{-6}$. However, the periodic state does not evolve toward chaos; rather it reverts back to a constant power state after exhibiting quasi-periodicity over a narrow range. It appears that the chaos is avoided because of the multimode nature of the laser. The laser enters the chaotic state at much higher feedback levels ($\sim 1 \cdot 10^{-4}$). In general, chaotic regions are much thinner compared to the single-mode case.

A question one may ask for the multimode case is how individual mode powers behave when the total power in all modes is chaotic. Specifically, the question is whether all modes follow chaotic oscillations in synchronization, or different modes oscillate independently. Synchronized chaos has been observed in the case of semiconductor laser arrays [25]. To answer this question, we look at the chaotic time series of individual modes in the chaotic window occurring near $F_{\text{ext}} = 1 \cdot 10^{-4}$ in Fig. 4(b). Figure 5 shows how the mode power evolved as F_{ext} was varied to follow the transition from periodic state to chaos, and then back to a periodic state. Unfortunately the possibility of synchronized chaos does not exist when spontaneous emission is turned off since almost all of the power is carried by one of the five modes (with extremely low-power side modes). In Figure 5(a) the CW state has just become unstable and the main-mode power is periodic at the relaxation-oscillation frequency. With a slight increase in F_{ext}, chaos sets in although all power is still in the main mode [Fig. 5(b)]. In Fig. 5(c), there is still chaos, but a miniscule amount of power has now gone into a side mode (it is too small to be seen on the scale used). With a slight increase in F_{ext} [Fig. 5(d)], the main and side modes have switched. The original main mode is now effectively off. Interestingly enough, the side mode emerges in a periodic state even though the main mode was in a chaotic state just before switching. This pattern of the transition from chaos to periodicity, corresponding to a switching of laser modes, repeats itself as feedback is increased. It will be seen in the

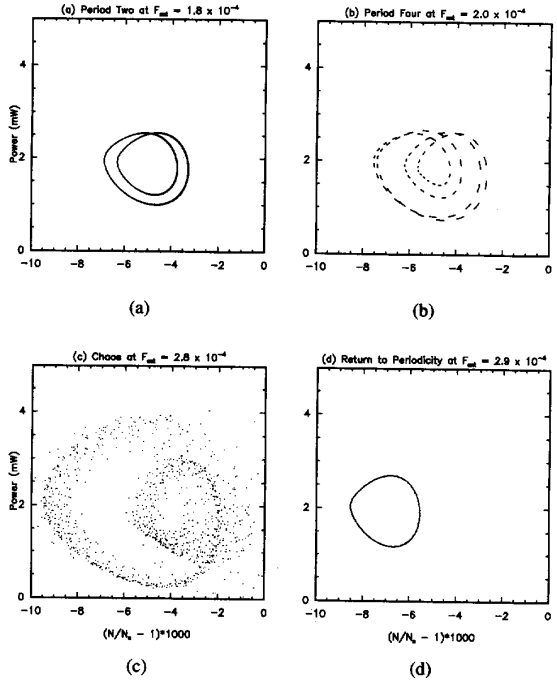

Fig. 6. Phase diagrams ($P_T - N$ trajectories) at four feedback levels, showing the onset of chaos through a period-doubling route and then transition back to a periodic state through mode switching.

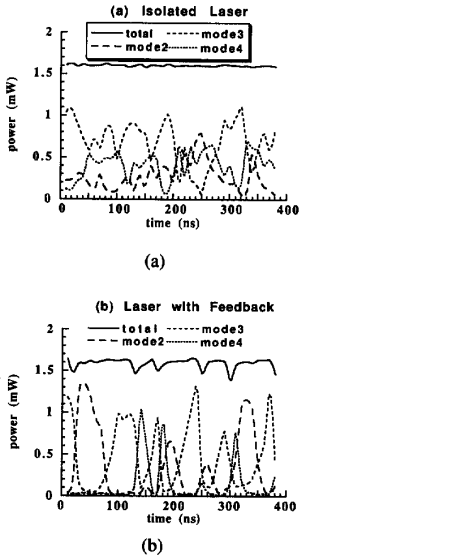

Fig. 7. Temporal variation of mode powers for (a) the solitary laser and (b) the same laser with feedback-induced chaos. Mode powers are averaged over a 10-ns window to remove fast oscillations associated with stochastic spontaneous emission noise.

next section that the laser exhibits random mode hopping in the chaotic region, and as a result is likely to end up in a different mode when it enters the stable nonchaotic regime.

These dynamical features can also be seen through the use of phase diagrams in which total output power is plotted as a function of carrier density for an entire trajectory. Figure 6 shows the laser in transition through periodic state to chaos and back. In Fig. 6(a) the double-loop indicates period doubling for $F_{\text{ext}} = 1.8 \cdot 10^{-4}$. A slight increase in F_{ext} leads in Fig. 6(b) to period-four oscillation. Figure 6(c) shows chaos occurring when F_{ext} is increased to $2.8 \cdot 10^{-4}$. However, as seen in Fig. 6(d), chaos ends, and the laser returns to single-period oscillation, when $F_{\text{ext}} = 2.9 \cdot 10^{-4}$. Note that the single loop in Fig. 6(d) is centered on a different point in $P-N$ space than the double-loop of Fig. 6(a), indicating that the operating conditions have changed because of mode switching. The next section discusses the mode-partition phenomenon with spontaneous emission included.

V. Effect of Spontaneous Emission on Chaos and Mode Spectra

In the discussion of OFB-induced chaos, we have so far neglected the role of spontaneous emission in order not to mix the effects of deterministic chaos with the stochastic noise. In practice, however, stochastic noise is always present in semiconductor lasers because of spontaneous emission and shot noise (resulting from generation and recombination of charge carriers). These noise sources are easily included in our multimode rate-equation model through the Langevin-noise terms $F_m(t)$ and $F_N(t)$ in (1) and (2). It turns out that $F_N(t)$ can be neglected since spontaneous emission dominates noise in semiconductor lasers. In this section we study OFB-induced chaotic dynamics by including the spontaneous-emission-induced noise with emphasis on mode partitioning. The noise level is determined by the rate of spontaneous emission rate R_{sp} through

$$\langle F_m^*(t) F_n(t') \rangle = R_{\text{sp}} \delta_{mn} \delta(t - t')$$

where the noise is assumed to be Markoffian (delta-correlated) and independent for each mode. The spontaneous emission rate depends on the cavity decay rate γ_m as $R_{\text{sp}} = n_{\text{sp}} \gamma_m$, where the spontaneous emission factor n_{sp} was chosen to be 1.8.

In the presence of spontaneous emission and appropriate OFB, the time series for mode powers exhibit stochastic fluctuations together with chaotic fluctuations. Since the power spectrum of stochastic fluctuations peaks at the relaxation-oscillation frequency, it is beneficial to the analysis to remove such high-frequency fluctuation of mode powers by performing a running average over a 10-ns window. The resulting time series is a measure of low-frequency mode-partition noise and reflects how a typical time-resolved spectrum of the laser would appear experimentally. Figure 7 shows the temporal variation of average mode powers for a solitary laser and for the same laser with OFB ($F_{\text{ext}} = 5 \cdot 10^{-4}$ and $L_{\text{ext}} = 10$ cm). The solitary laser [Fig. 7(a)] exhibits mode-partition fluctuations, but remains multimoded most of the time. In contrast, Fig. 7(b) shows that the laser is essentially single-moded all the time, but the laser exhibits mode hopping at random times. The total power of a solitary laser is nearly constant [Fig. 7(a)], while it exhibits large fluctuations in the presence of OFB [Fig. 7(b)]. These low-frequency fluctuations are indicative of OFB-induced chaos. From a

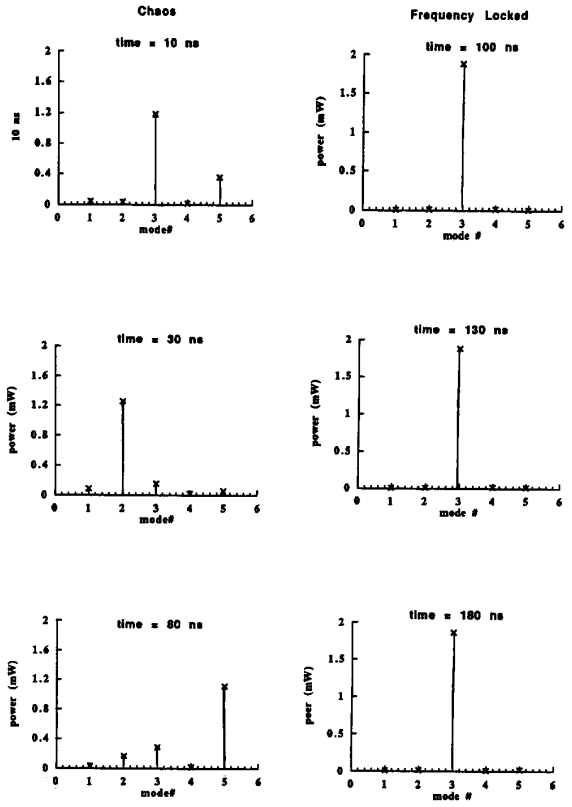

Fig. 8. Time-resolved mode spectra at three different times for a multimode laser with feedback in the chaotic region (left column) and in the nonchaotic region (right column). The dominant mode switches wavelength among various modes in the chaotic region (wavelength fluctuations), but stays at the same wavelength in the nonchaotic region.

practical standpoint, the low-frequency laser RIN appears to be enhanced by a large amount (> 20 dB) because of OFB. From a fundamental standpoint, this RIN enhancement is due to the appearance of chaos that induces random mode hops in a multimode laser. In fact, it should not even be called RIN enhancement because the increase in low-frequency noise is deterministic in nature whereas RIN normally refers to the stochastic intensity noise. Mode hopping occurs only when the OFB level corresponds to a chaotic window in the bifurcation diagram [Fig. 4(b)]. For a nonchaotic feedback level, the multimode laser remains in a single longitudinal mode over long periods of time since mode hopping does not occur. Figure 8 shows mode spectra in the chaotic (left column) and nonchaotic (right column) regions. In the chaotic case, the laser jumps from one mode to another mode randomly. By contrast, the laser stays in the same mode in the nonchaotic case. To explain why this happens, we return to the bifurcation diagram.

With the spontaneous emission included in the model, the bifurcations are more difficult to discern since stochastic noise appears as a thick band even without OFB when the laser is operating continuously. The lower plot in Fig. 9 shows the bifurcation diagram for the laser with five modes and $L_{\text{ext}} = 10$ cm (with spontaneous emission included). The regions of chaos are still quite distinguishable since the chaos

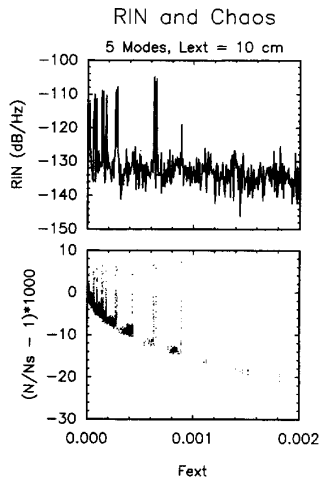

Fig. 9. (a) Low-frequency RIN versus F_{ext} for a multimode laser. (b) The corresponding bifurcation diagram. The RIN is enhanced by as much as 20 dB within each chaotic window.

introduces much larger deviations in the total power P_T and the carrier number N than those introduced by spontaneous emission. Figures 8(a)–(c) show the mode powers in such a chaotic region, while Figs. 8(d)–(f) are taken from a region where there is no chaos, only stochastic spontaneous emission noise.

The upper curve in Fig. 9 shows the variation of low-frequency RIN (averaged over the 0–100-MHz range) as a function of F_{ext}. There is one-to-one correspondence between the regions of chaos and the regions of high RIN. This clearly demonstrates that deterministic chaos is the cause of the high RIN levels observed in semiconductor lasers in the presence of optical feedback. Since the location and the width of chaotic windows depend on many laser parameters, such as the linewidth enhancement factor α and the nonlinear gain parameter ϵ, the variation of low-frequency RIN with the OFB level also depend strongly on these parameters. Figure 10 shows the low-frequency RIN as a function of the OFB level R_{ext} for several values of the linewidth enhancement factor α in the range 0–6 by assuming 2% coupling efficiency ($\eta_c - 2\%$). The RIN is nearly independent of α for $\alpha < 2$ since chaos does not occur for such low values of α. However, it is significantly enhanced for $\alpha = 4$ and 6 for OFB levels that correspond to the chaotic windows in the bifurcation diagram. Figure 11 shows the dependence of RIN on the nonlinear gain parameter ϵ. As discussed in Section III for the single-mode case, chaos almost disappears for large values of ϵ. As a result, the RIN becomes almost independent of F_{ext} for large values of ϵ. The next section considers a means of controlling the chaos and hence reducing the feedback-induced noise in semiconductor lasers.

VI. Control of Feedback-Induced Chaos

As mentioned in the Introduction, the HFI technique involving sinusoidal modulation of the drive current has been used with some success in reducing the RIN of semiconductor

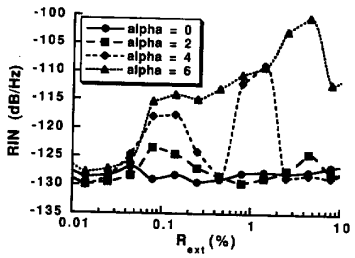

Fig. 10. Dependence of low-frequency RIN enhancement on the linewidth enhancement factor α.

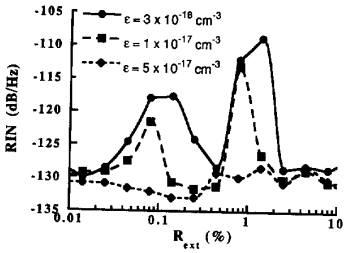

Fig. 11. Dependence of low-frequency RIN enhancement on the nonlinear gain parameter ϵ.

lasers in optical recording systems [16]–[22]. Since the RIN enhancement is in fact due to the onset of deterministic chaos, it follows that the RIN can be reduced only if current modulation eliminates optical chaos. This section considers the effect of OFB in directly modulated multimode semiconductor lasers. For this purpose, the multimode rate equations (1) and (2) are integrated numerically by replacing the drive current I in (2) by

$$I(t) = I_b + I_m \sin(2\pi f_m t) \tag{8}$$

where I_b is the bias current, I_m is the modulation current, and f_m is the frequency of sinusoidal modulation.

Figure 12(a) shows the variation of low-frequency RIN with the OFB level for modulation frequencies of 275 and 500 MHz. The unmodulated case ($f_m = 0$ MHz) is included for reference in Fig. 12(a). Although RIN is reduced for $f_m = 275$ MHz, the choice of 500 MHz is much better since the RIN is close to the solitary-laser value over a large range of OFB. As observed also experimentally [20], the ability to suppress the RIN enhancement is sensitive to the choice of the modulation frequency. One may ask what modulation frequency is the best for control of chaos. This answer depends critically on the length of the external cavity. In the long external cavity limit ($\nu_{ext} < \nu_R$) modulation at a frequency near $\nu_{ext}/2$ appears to work well, since the laser is essentially turned off at the time the OFB returns to the laser [16]. For short external cavities, however, this simple formula does not work as well. Instead, to determine the optimum modulation frequency, the low-frequency RIN is plotted in Fig. 12(b) as a function of modulation frequency for three different feedback levels, chosen such that they cover both chaotic windows and the nonchaotic region between them. For this particular laser the

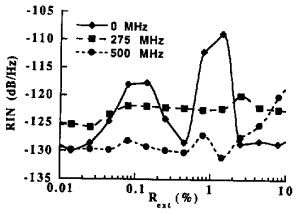

(a)

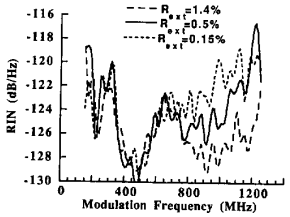

(b)

Fig. 12. Dependence of low-frequency RIN on modulation frequency. (a) RIN versus OFB for three modulation frequencies (b) RIN versus modulation frequency for three values of OFB levels. Modulation current is 20 mA (peak-to-peak).

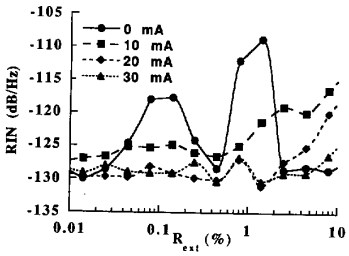

Fig. 13. RIN versus OFB for three values of the modulation currents (peak-to-peak) at a modulation frequency of 500 MHz. The unmodulated case is also shown for comparison.

optimum modulation frequency appears to be 480 MHz. The RIN suppression is also sensitive to modulation current. Figure 13 shows the RIN as a function of peak-to-peak modulation current ($2I_m$) when the modulation frequency is chosen to be at its optimum value of 480 MHz. The chaotic windows are eliminated only when the current is modulated such that the laser is driven below threshold over a part of the modulation cycle. The lowest values of RIN occur for relatively large values of I_m chosen such that the laser is driven considerably below threshold. These results demonstrate that it is possible to eliminate the feedback-induced RIN enhancement over a broad range of feedback levels by using the HFI technique.

We can gain an understanding of this phenomenon by investigating the laser dynamics under optimum modulation conditions. An important question is how current modulation affects the mode spectra. Figure 14 shows the mode powers averaged over 10 ns, analogous to those shown in Figs. 7 and 8, for a multimode laser modulated at 480 MHz with $I_m = 10$ mA. Current modulation has the effect of spreading the total power more or less evenly among the laser modes over a time scale longer than 10 ns. On a shorter time scale, shown in Fig. 15, where the individual mode powers together with

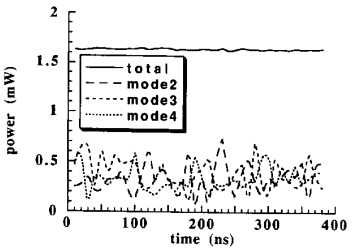

Fig. 14. Temporal variation of mode powers under condition identical to those of Fig. 7(b) except that the semiconductor laser is modulated at 500 MHz.

the total power are plotted as a function of time, all modes appear to oscillate at the modulation frequency. Furthermore, the oscillation amplitude varies randomly from cycle to cycle. An interesting question is whether the random amplitudes of the mode powers oscillating at the modulation frequency are chaotic or stochastic in nature. This question can be answered by noting that the low-frequency RIN is near the solitary-laser value for the time series shown in Fig. 15. Since a hallmark sign of chaos is the appearance of broadband noise, the absence of such a noise indicates that the random oscillations in Fig. 15 are stochastic in nature. Physically, the mode powers grow from the seed provided by spontaneous emission when the laser goes below threshold during each cycle, and all modes have equal probability of being excited. Thus, even though the total peak power is nearly constant from cycle to cycle [see Fig. 15(d)], individual mode powers fluctuate wildly. Such mode partitioning is certainly stochastic in nature.

It is clear from the above discussion that current modulation such that the laser goes below threshold during each cycle helps to eliminate feedback-induced chaos. One may ask over what range of OFB levels such a suppression of chaos can occur. This question can be answered through a bifurcation diagram. Figure 16 shows the bifurcation diagram under conditions identical to those of Fig. 4(b) except that the laser is modulated at the optimum frequency of 480 MHz and spontaneous emission is included through the Langevin terms in the multimode rate equations. The band-like appearance is due to stochastic noise and should not be confused with quasi-periodicity. The important point to note is that the feedback-induced chaos is suppressed for feedback levels as large as $F_{\text{ext}} \sim 2 \cdot 10^{-3}$. Compared to the unmodulated case shown in Fig. 4(b), the onset of chaos is delayed by well over an order of magnitude when the laser is modulated.

The optimum modulation frequency of 480 MHz found in numerical simulations is specific to the laser under consideration. One may ask how this frequency will change from laser to laser. In particular, can one establish guidelines to estimate this frequency? Such guidelines exist [16] for relatively long external cavities ($L > 30$ cm) for which $\nu_{\text{ext}} < \nu_R$. The modulation frequency f_m should be chosen such that the laser is turned off when the feedback returns to the laser cavity. This condition can be satisfied by choosing f_m close to $\nu_{\text{ext}}/2$. Unfortunately this simple recipe does not work for short cavities for which $\nu_{\text{ext}} > \nu_R$. One of the reasons is that $\nu_{\text{ext}}/2$ may lie close to ν_R, an undesirable situation since modulation near the relaxation-oscillation frequency can destabilize the laser. Experimental data indicate that the optimum modulation frequency varies from laser to laser with values generally lying in the range $\nu_{\text{ext}}/2 < f_m < \nu_{\text{ext}}$. In fact, the primary objective of this work was to predict f_m numerically so that such simulations can be used as a computer-aided design tool for optical recording systems. In the next section we present the experimental data on the specific laser whose parameters were used in the numerical simulations. An agreement between simulations and experiments helps to validate the computer model.

VII. Experimental Results

To compare the theoretical predictions with experiments, we have carried out measurements of the low-frequency RIN of an optical recording diode laser as a function of OFB using a range of modulation frequencies and depths. As in the simulations, the external cavity length is 10 cm. The OFB level is varied in the range of 0.1–10%, while the laser power is kept constant at 1.6 mW. In the experimental plots, each data point represents an average of the measurements of 10 identical lasers; the error bars correspond to the standard deviation of this sample of 10 lasers. By measuring the small-signal modulation response, we have determined that only approximately 60% of the modulation current at 500 MHz is effective in driving the laser. This should be kept in mind when comparing the modulation currents employed experimentally with those of the simulations. Figure 17 shows RIN versus OFB for several different modulation frequencies, using a modulation current of 40 mA (peak-to-peak). Of the five modulation frequencies shown, 480 MHz results in by far the greatest suppression of the RIN enhancement: the RIN remains below -125 dB/Hz up to 5% OFB. Recall that the computer simulations predict (see Fig. 12) that a modulation frequency in the range 450–500 MHz gives the lowest values of RIN. Typical two-sided error bars for this plot are 3–4 dB.

The next experimental result, shown in Fig. 18, shows RIN versus OFB for different modulation currents, using the modulation frequency of 480 MHz. The modulation currents shown are peak-to-peak values and are similar to the values used in the simulations. The unmodulated case is shown for comparison. The similarity of the experimental measurements to the simulated results in Fig. 13 is quite apparent. With no modulation, the experimental RIN has already increased to high values for a feedback of 0.1%, similar to the simulations. At high feedback levels, the experimental RIN can actually decrease to low values when OFB lies between two chaotic windows, as seen in the simulations [see Fig. 4(b)]. Experimentally, the high-feedback regime is very unstable, and the RIN fluctuates between high and low values. A typical error bar shown on the unmodulated RIN curve is 10 dB for OFB levels > 1%. This is consistent with Fig. 4(b), where multiple chaotic windows are seen to occur. When current modulation is turned on, the RIN becomes low and approaches the solitary-laser value, in agreement with the numerical simulations (see Fig. 13). Larger modulation depths are more effective in

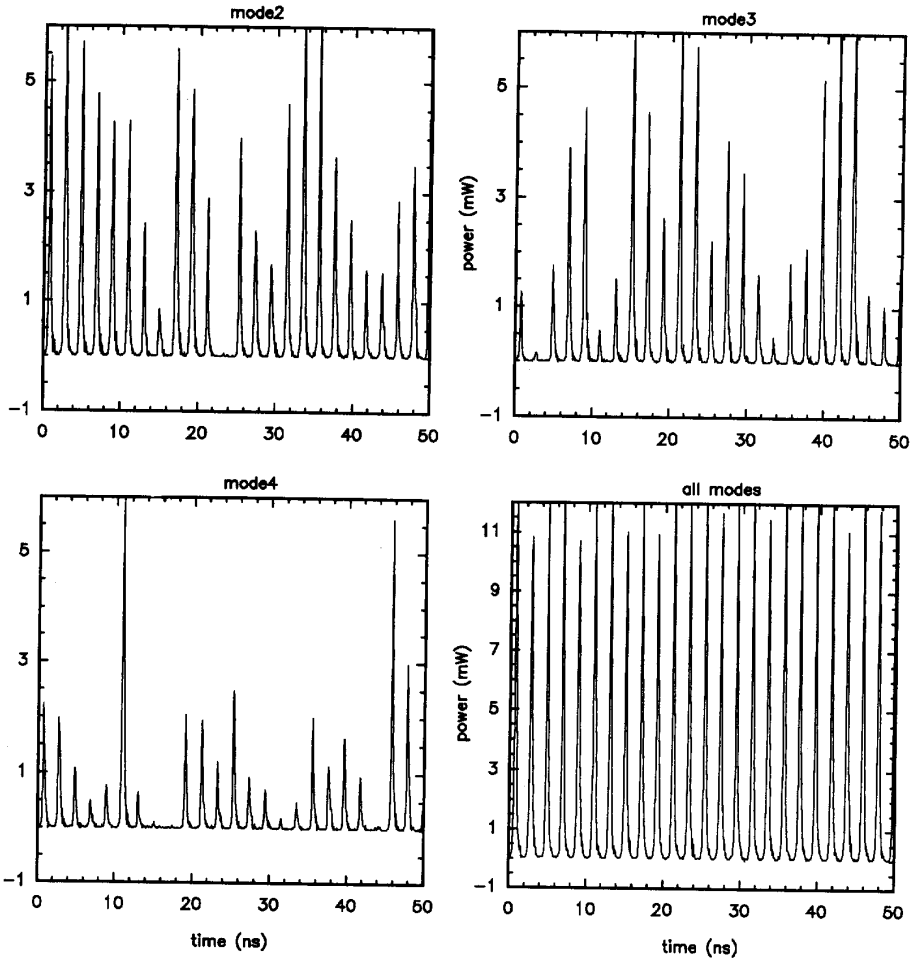

Fig. 15. Temporal variation of mode powers at a feedback level within a chaotic window in Fig. 4(b).

delaying the onset of chaos, again in agreement with computer simulations.

VIII. Conclusions

Semiconductor lasers in the presence of external optical feedback exhibit an enhancement of low-frequency RIN that is detrimental to some system applications such as optical data recording. Based on the results presented here, one can conclude that this RIN enhancement is due to the onset of deterministic chaos whenever the feedback level lies within a chaotic window of the bifurcation diagram. We have integrated the multimode rate equations numerically to determine the location of such chaotic windows. It turns out that the OFB range over which the laser becomes chaotic is sensitive to several parameters. The most important among them are i) external cavity length L_{ext}, ii) linewidth enhancement factor α, and iii) nonlinear gain ϵ. We have discussed the dependence of chaotic dynamics and the associated enhancement of the low-frequency RIN on these three parameters in detail.

A new feature of multimode chaos is the dependence of mode spectra on the OFB level. We have found that OFB in multimode lasers generally forces the laser to oscillate in a single longitudinal mode, although the dominant mode is not always the same. In fact, chaos in multimode lasers is accompanied by mode hopping. When the laser output becomes chaotic, the laser hops from mode to mode apparently randomly. Further increase in the OFB level may return the laser to a periodic state, and mode hopping stops.

A solution of the RIN enhancement problem is provided by modulation of the injection current. With the proper choice of modulation frequency and current, the onset of deterministic chaos, and consequently the enhancement of the low-frequency RIN, can be delayed by more than an order of magnitude so that it occurs at much higher feedback levels. Current modulation forces the laser to go below threshold during each modulation cycle. Since the mode powers grow from noise in the below-threshold regime, spontaneous emission and the associated stochastic noise dominate the dynamics of a modulated multimode semiconductor laser. Numerical

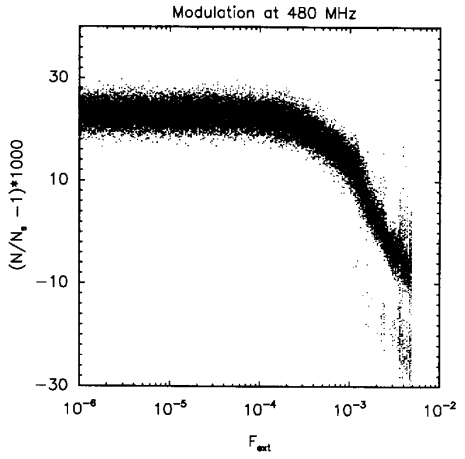

Fig. 16. Bifurcation diagram for a multimode semiconductor laser under conditions identical to those of Fig. 4(b) except that spontaneous emission is included and that the laser is modulated at the optimum modulation frequency of 480 MHz.

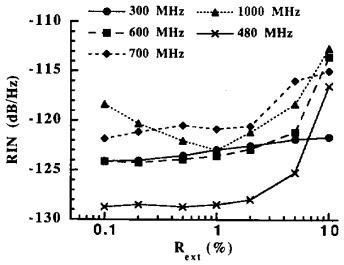

Fig. 17. Experimental measurement of RIN versus OFB for five different modulation frequencies. Modulation current is 40 mA peak-to-peak.

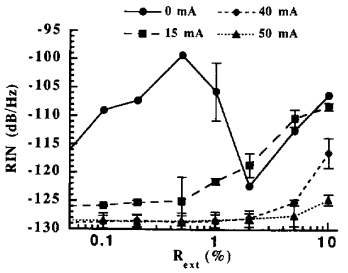

Fig. 18. Experimental measurement of RIN versus OFB for three different modulation currents. The unmodulated case is also shown for comparison.

simulations indicate that mode switching is eliminated in this case simply because all modes carry roughly equal powers on a time scale much longer than the modulation period. In essence, current modulation forces the laser to become multimoded, and in the process eliminates the chaos. The current-modulation technique has application in optical data recording systems since its use reduces the laser noise even in the presence of OFB from the optical disk [20]–[22].

ACKNOWLEDGMENT

We thank Scott Beckens for assistance with the experimental measurements and Dave Kay for technical advice.

REFERENCES

[1] G. P. Agrawal and N. K. Dutta, *Semiconductor Lasers*, 2nd ed. New York: Van Nostrand Reinhold, 1993.
[2] K. Petermann, *Laser Diode Modulation and Noise* . Boston: Kluwer Academic, 1991.
[3] D. Lenstra, B. H. Verbeek, and A. J. den Boef, "Coherence collapse in single-mode semiconductor lasers due to optical feedback," *IEEE J. Quantum Electron.*, vol. QE-21, pp. 674–679, 1985.
[4] R. W. Tkach and A. R. Chraplyvy, "Regimes of feedback effects in 1.5-μm distributed feedback lasers," *J. Lightwave Technol.*, vol. LT-4 pp. 1655–1661, 1986.
[5] G. C. Dente, P. S. Durkin, K. A. Wilson, and C. E. Moeller, "Chaos in the coherence collapse of semiconductor lasers," *IEEE J. Quantum Electron.*, vol. 24, pp. 2441–2447, 1988.
[6] N. Schunk and K. Petermann, "Numerical analysis of the feedback regimes for a single-mode semiconductor laser with external feedback," *IEEE J. Quantum Electron.*, vol. 24, pp. 1242–1247, 1988.
[7] J. Sacher, W. Elsässer, and E. O. Göbel, "Intermittency in the coherence collapse of a semiconductor laser with external feedback," *Phys. Rev. Lett.*, vol. 63, pp. 2224–2227, 1989.
[8] B. Tromborg and J. Mork, "Stability analysis and the route to chaos for laser diodes with optical feedback," *IEEE Photon. Technol. Lett.*, vol. 2, pp. 549–552, 1990.
[9] J. Mork, J. Mark, and B. Tromborg, "Route to chaos and competition between relaxation oscillations for a semiconductor laser with optical feedback," *Phys. Rev. Lett.*, vol. 65, pp. 1999–2002, 1990.
[10] J. S. Cohen, F. Wittgrefe, M. D. Hoogerland, and J. P. Woerdman, "Optical spectra of semiconductor lasers with incoherent optical feedback," *IEEE J. Quantum Electron.*, vol. 26, pp. 982–990, 1990.
[11] J. D. Park, D. S. Seo, and J. G. McInerney, "Self-pulsations in strongly coupled asymmetric external cavity semiconductor lasers," *IEEE J. Quantum Electron.*, vol. 26, pp. 1353–1362, 1990.
[12] D. Lenstra, "Statistical theory of the multistable external feedback lasers," *Opt. Commun.*, vol. 81, pp. 209–214, 1991.
[13] J. Wang and K. Petermann, "Noise analysis of semiconductor lasers within coherence collapse region," *IEEE J. Quantum Electron.*, vol. 27, pp. 3–9, 1991.
[14] J. Sacher, W. Elsässer, and E. O. Göbel, "Nonlinear dynamics of semiconductor lasers under variable feedback conditions," *IEEE J. Quantum Electron.*, vol. 27, pp. 373–379, 1991.
[15] J. Mork, B. Tromborg, and J. Mark, "Chaos in semiconductor laser with optical feedback: Theory and experiment," *IEEE J. Quantum Electron.*, vol. 28, pp. 93–108, 1992.
[16] T. Kanada, "Theoretical study of noise reduction effects by superimposed pulse modulation," *Trans. IECE Jpn.*, vol. 68, pp. 180–185, 1985.
[17] K. Stubkjaer and M. B. Small, "Feedback-induced noise in index-guided semiconductor lasers and its reduction by modulation," *Electron. Lett.*, vol. 19, pp. 388–389, 1983.
[18] A. Arimoto, M. Ojima, N. Chinone, A. Oishi, T. Gotoh, and N. Ohnuki, "Optimum conditions for the high frequency noise reduction method in optical videodisc players," *Appl. Opt.*, vol. 25, pp. 1398–1403, 1986.
[19] M. Ojima, A. Arimoto, N. Chinone, T. Gotoh, and K. Aiki, "Diode laser noise at video frequencies in optical videodisc players," *Appl. Opt.*, vol. 25, pp. 1404–1410, 1986.
[20] E. C. Gage and S. Beckens, "Effects of high frequency injection and optical feedback on semiconductor laser performance," *SPIE Optical Data Storage*, vol. 1316, pp. 199–204, 1990.
[21] M. Yamada and T. Higashi, "Mechanism of the noise reduction method by superposition of high-frequency current for semiconductor injection lasers," *IEEE J. Quantum Electron.*, vol. 27, pp. 380–388, 1991.
[22] G. R. Gray, A. T. Ryan, G. P. Agrawal, and E. C. Gage, "Control of optical-feedback-induced laser intensity noise in optical data recording," *Opt. Eng.*, vol. 32, pp. 739–745, 1993.
[23] R. Lang and K. Kobayashi, "External optical feedback effects on semiconductor injection laser properties," *IEEE J. Quantum Electron.*, vol. QE-16, pp. 347–355, 1980.
[24] G. P. Agrawal, "Gain nonlinearities in semiconductor lasers: theory and application to distributed feedback lasers," *IEEE J. Quantum Electron.*, vol. QE-23, pp. 860–870, 1987.
[25] H. G. Winful and L. Rahman, "Synchronized chaos and spatio-temporal chaos in arrays of coupled lasers," *Phys. Rev. Lett.*, vol. 65, pp. 1575–1578, 1990.

Andrew T. Ryan received his B.S. degree from the State University of New York College at Oswego, where he studied physics and mathematics. He has performed undergraduate research in optics at the Chemical Physics Institute at the University of Oregon in Eugene. He is currently working toward his Ph.D. degree with Dr. Govind Agrawal at the Institute of Optics at the University of Rochester in Rochester, New York.

Govind P. Agrawal (M'83–SM'86) received the B.S. degree from the University of Lucknow in 1969 and the M.S. and Ph.D. degrees from the Indian Institute of Technology, New Delhi, in 1971 and 1974, respectively.

After holding positions at the Ecole Polytechnique, France, the City University of New York, and AT&T Bell Laboratories, Murray Hill, Dr. Agrawal joined the faculty of the Institute of Optics at the University of Rochester, where he is a professor of optics. His resea4rch interests focus on quantum electronics, nonlinear optics, and laser physics. In particular, he has contributed significantly to the fields of semiconductor lasers, nonlinear fiber optics, and optical communications. He is an author or coauthor of more than 180 research papers, several bok chapters and review articles, and three books, entitled *Semiconductor Lasers* (Van Nostrand Reinhold), *Nonlinear Fiber Optics* (Academic Press), and *Fiber-Optic Communication Systems* (Wiley). He also coedited the book *Contemporary Nonlinear Optics* (Academic Press).

Dr. Agrawal is a fellow of the Optical Society of America and a senior member of the Institute of Electrical and Electronics Engineers.

George R. Gray (M'93) received a B.A. degree in math and physics from Hanover College, and M.S. and Ph.D. degrees in physics from the Georgia Institute of Technology in 1985, 1987, and 1990, respectively. Through 1992 he was a research associate at the Institute of Optics, University of Rochester. Since December 1992 he has been an assistant professor in the Electrical Engineering Department of the University of Utah. His interests include instabilituie3s and nonlinear dynamics in semiconductor lasers and the application of semiconductor lasers to optical recording and optical communications. Dr. Gray is a member of IEEE and the Optical Society of America.

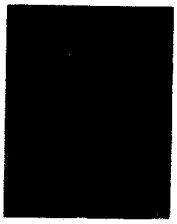

Edward C. Gage received the B.A. degree in physics from the State University of New York at Geneseo in 1983 and the M.A. and Ph.D. degrees in physics from the University of Rochester, in 1985 and 1989, respectively. The topic of his doctoral research was intensity fluctuations in one- and two-mode dye lasers.

He has been with Eastman Kodak Company since 1989 as a research scientists in the Storage Technology Research and Development Division. His research interests are in the areas of semiconductor laser physics and optical recording.

Dr. Gage is a member of the OSA and IEEE Lasers and Electro-Optics Society.